Materials Today Communications 51 (2026) 114751

Contents lists available at ScienceDirect

Materials Today Communications

journal homepage: www.elsevier.com/locate/mtcomm

Hardening by annealing in the medium-entropy alloy CrCoNi after equal-channel angular pressing

Lisa-Marie Rymer [a,*], Heinz Werner Höppel [b], Patrick Ortner [b], Nina Pfeffer [b], Andreas Stark [c], Lisa Winter [a], Thomas Lampke [a]

[a] Institute of Materials Science and Engineering, Materials and Surface Engineering Group, Chemnitz University of Technology, 09107 Chemnitz, Germany
[b] Friedrich-Alexander Universität Erlangen-Nürnberg, FAU, Dept. Materials Science & Engineering, Institute 1, Martensstraße 5, Erlangen, 91058 Bavaria, Germany
[c] Helmholtz-Zentrum Hereon, Geesthacht, Germany

ARTICLE INFO

Keywords:
Anneal-induced hardening
CrCoNi
Equal-channel angular pressing
Heat treatment
Microstructural characterization

ABSTRACT

After equal-channel angular pressing (ECAP) and a subsequent heat treatment at 600 °C for 1 h, the MEA CrCoNi is characterized by a yield strength of about 1.4 GPa but a drastically low uniform elongation of 1.2 %. High-energy X-ray diffraction analysis, transmission electron microscopy, and high-resolution high-angle annular dark-field scanning transmission electron microscopy investigations were performed, but the cause of the annealing-induced hardening could not be conclusively determined, although differential scanning calorimetry measurements reveal an exothermic peak and thus microstructural changes in the temperature range between 450 °C and 650 °C. Despite the complex nature of the MEA CrCoNi, the dominant deformation mechanisms after ECAP processing and a subsequent heat treatment during straining appear to be similar to those of conventional alloys. It is assumed that the rearrangement of dislocations in low-energy configurations and, to some extent, grain and twin boundary relaxation lead to the anneal-induced hardening effect at 600 °C. Grain boundary dislocations are hindered from bowing out or activating new dislocation sources, resulting in the strong increase in yield and ultimate tensile strength.

1. Introduction

The medium-entropy alloy (MEA) CrCoNi (each 33.3 at.-%) is known for its exceptional combination of high strength and high ductility at room and cryogenic temperatures [1,2], high fracture toughness [3,4], high corrosion resistance [5] and high oxidation resistance in air [6]. These properties are probably due to the equiatomic chemical composition of the alloying elements, which makes MEAs unique compared to conventional alloys. The complex nature of CrCoNi is attributed to the so-called core effects: a medium to high configurational entropy, sluggish diffusion, a higher lattice distortion than conventional alloys, and the cocktail effect, which are described in detail in the literature [7,8]. In addition, if the single face-centered cubic (fcc) CrCoNi is recrystallized, it can be easily plastically deformed to obtain high degrees of deformation. Therefore, CrCoNi can be processed using severe plastic deformation (SPD) techniques. In literature, CrCoNi has been processed by cold rolling [9,10], asymmetric cryorolling [11,12], equal-channel angular pressing (ECAP) [13–15], and high-pressure torsion [16,17]. SPD of CrCoNi significantly improves yield (YS) and ultimate tensile strength (UTS) [13,15,17]. However, ductility is strongly reduced. The predominant strengthening mechanisms are dislocation and grain boundary hardening due to the high number of dislocations introduced and the reduced grain size after SPD [18]. Since CrCoNi exhibits a low stacking fault energy (SFE) of about 22 ± 4 mJ/m^2 [1], stacking faults (SFs) and deformation twins also form and phase transformations could be activated in addition to dislocation motion [1,12,19]. The formation of these microstructural elements is forced at high strains [1,20], at high strain rates [21], and at low/cryogenic temperatures [1,19,20,22,23]. After SPD of CrCoNi, a subsequent heat treatment is often performed in order to regain a certain degree of ductility, as point defects heal and dislocations are rearranged in low-energy configurations or annihilate [9,13,24]. However, a heat treatment at 500°C to 600 °C in CrCoNi after cold rolling [9,25], ECAP [13–15] and HPT [24] forms a hcp-phase at deformation twins. In general, the hcp-phase is only a few atomic layers thick, as a partial dislocation glides on an adjacent plane of a deformation twin to form the hcp stacking sequence, which grows with the

* Corresponding author.
E-mail addresses: lisa-marie.rymer@mb.tu-chemnitz.de (L.-M. Rymer), hwe.hoeppel@fau.de (H.W. Höppel), patrick.p.ortner@fau.de (P. Ortner), nina.pfeffer@fau.de (N. Pfeffer), andreas.stark@hereon.de (A. Stark), lisa.winter@mb.tu-chemnitz.de (L. Winter), thomas.lampke@mb.tu-chemnitz.de (T. Lampke).

https://doi.org/10.1016/j.mtcomm.2026.114751
Received 23 October 2025; Received in revised form 22 January 2026; Accepted 28 January 2026
Available online 29 January 2026

activation of further partial dislocations on second neighboring planes [20,26]. The formation of a hcp-phase is favored because it has a lower energy than the fcc phase [19,26] and to reduce lattice distortion [14]. Due to the change in the stacking sequence at the deformation twins after plastic deformation and heat treatment in CrCoNi, an increase in hardness and strength was observed [10,13,14]. However, not all publications mention the formation of an hcp-phase as the origin of the increase in strength in CrCoNi. Other reasons for anneal-induced hardening could be segregations/short-range ordering (SRO) [27–29], grain boundary relaxation [16,30–33], after a combination of SPD and a subsequent heat treatment [34], and/or the interaction of mobile dislocations with forest dislocations [30,35]. The origin of SRO is the magnetic frustration of parallel spin pairs [36]. Magnetic frustration occurs when ferromagnetic elements such as Co and Ni are alloyed next to non-ferromagnetic elements such as Cr [37]. The elements interact with each other, generating favored pairs. In CrCoNi, Co-Cr pairs and Ni segregations [27,38,39] as well as Ni-Cr and/or Cr-Cr pairs [40,41] are formed. In contrast, grain boundary relaxation is characterized by a decrease in the number of grain boundary dislocation sources [32], which leads to an impeded formation of new dislocations and thus to an increase in material's strength [42]. This anneal-induced hardening is often observed in ultrafine-grained materials due to their initial high dislocation density and small grain size. In addition, low-temperature annealing in ultrafine-grained materials results in the annihilation of mobile dislocations, which further hardens the material [43]. Another reason for anneal-induced hardening is the formation of jogs due to the interaction of mobile and forest dislocations [35]. Jogs effectively hinder dislocation glide, resulting in an increase in strength. Finally, Mompiou et al. [44] found that dislocations become immobile if they are fully incorporated in grain boundaries during unloading, leading to lattice distortions and a corresponding stress field and thus an increase in yield strength.

In this study, the influence of ECAP processing and a subsequent heat treatment on the microstructure and the quasi-static tensile deformation behavior of the MEA CrCoNi was investigated. In order to reveal relevant phase transformations and deformation mechanisms, a combination of thermoanalytical (differential scanning calorimetry), crystallographic (X-ray diffraction), mechanical (quasi-static tensile tests), and imaging techniques (transmission electron microscopy) was used. Despite these manifold techniques used, the microstructural reasons for the observed annealing-induced hardening are hard to identify. However, it is suggested that the rearrangement of dislocations in low-energy configurations and, to some extent, grain and twin boundary relaxation lead to the anneal-induced hardening effect at 600 °C. It seems that a higher stress is needed to bow out grain boundary dislocations and to activate new dislocation sources, which results in an increase in YS and UTS.

2. Material and experimental methods

2.1. Material preparation

Pure elements of Cr (99.95 %), Co (99.9 %) and Ni (99.95 %) were melted using vacuum induction melting by Hauner GmbH und Co. KG (Röttenbach, Germany). The CrCoNi ingots thus produced were then homogenized at 1150 °C for 6 h in a vacuum furnace (Torvac 12 Mark IV, Minneapolis, Minnesota, USA). After homogenization, the ingots were hot forged using a 100 t hydraulic press at CMMC GmbH, Chemnitz. The ingots were preheated to 1200 °C for 30 min (Linn High Therm laboratory chamber furnace, Eschenfelden, Germany) before forging. The die was additionally heated to avoid edge cracks on the ingots. After hot forging, the ingots were recrystallized at 900 °C for 2 h (Linn High Therm, muffle furnace, Eschenfelden, Germany) under argon and subsequently cooled in air. The condition thus produced is further denoted as "C0".

2.2. ECAP processing

ECAP was carried out using a tool with a channel angle of 120°. To reduce friction, the ECAP tool is equipped with moveable channel walls. The induced strain per ECAP pass is about 0.68 [45], which leads to a total induced strain of about 2.04 after three ECAP passes. ECAP billets with a cross-section of 15 mm × 15 mm were processed with a pressing speed of 20 mm/min three times using route C [46], which is characterized by the rotation of the billets by 180° each pass. The ECAP-processed condition is further denoted as "C3". In addition, $MoSi_2$ was used as a lubricant. Furthermore, the ECAP tool was heated to 300° C to improve the formability of CrCoNi, as previous studies show that it is severely prone to cracking at the edges when pressing at room temperature. The higher processing temperature leads to recovery processes during ECAP processing, resulting in sufficient residual formability for multiple passes.

2.3. Differential scanning calorimetry measurements of condition C3 and subsequent heat treatment

After three ECAP passes, condition C3 was analyzed by differential scanning calorimetry (DSC). DSC measurements are used to determine phase transitions as a function of temperature. Particularly for highly deformed materials, (re-)crystallization processes can be detected additionally. DSC measurements were conducted using the simultaneous thermal analyzer STA 449 (NETZSCH-Gerätebau GmbH, Selb, Germany). The cylindrical specimens (d = 5 mm, h = 2 mm) of condition C3 were heated three times to 1000 °C and cooled to 100 °C to study the differences between the first and the following cycles. The specimens were placed in a crucible made of Al_2O_3. The reference crucible was left empty. The specimens were heated and cooled at a rate of 20 K/min. The tests were performed under an argon atmosphere. Resulting from the DSC measurements, condition C3 was heat treated at 600 °C for 1 h under an argon atmosphere using a muffle furnace (VMK80, Linn High Temp GmbH, Eschenfelden, Germany). The obtained condition is further denoted as "C3, 600 °C, 1 h".

2.4. High-energy X-ray diffraction measurements

The phase composition of the studied conditions was determined by high-energy X-ray diffraction (HEXRD) measurements with the radiation source PETRA III at the research center DESY in Hamburg, beamline P07, which is operated by Hereon (proposal I-20230881). The X-ray energy used was 103.3 keV ($\lambda = 0.120$ Å). The beam spot size was 1 mm x 1 mm. In addition, a PerkinElmer area detector with a pixel size of 200 µm x 200 µm was used. The sample-to-detector distance was set to 1630 mm. The material was analyzed in the Z-direction, see Fig. 1.

2.5. Mechanical and microstructural characterization

To determine the mechanical parameters, quasi-static tensile tests were conducted. The used dog-bone-shaped tensile specimens (cross-section of 2 mm × 1.5 mm and a gauge length of 5 mm) were tested with

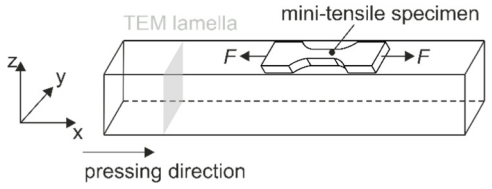

Fig. 1. Schematic illustration of the equal-channel angular pressing (ECAP) billet. The pressing direction (parallel to the length axis of the die's exit channel), the position and loading direction of the mini-tensile specimens, and the plane for the TEM investigations are marked.

a 20 kN standard tensile testing machine (Allround-Line) from Zwick-Roell (ZwickRoell GmbH & Co KG, Ulm, Germany). The dog-bone-shaped tensile specimens were extracted from the ECAP billet as shown in Fig. 1. The loading direction was in the pressing direction (Fig. 1). The tests were performed with an initial strain rate of $\dot{\varepsilon} = 10^{-3}$ s^{-1} at room temperature. To determine the strain, digital image correlation (GOM Aramis, Carl Zeiss GOM Metrology GmbH, Braunschweig, Germany) was used. For each condition, seven specimens were tested.

For electron backscatter diffraction (EBSD) measurements, cross-sections of each condition were prepared in Z-plane, see Fig. 1. Each cross-section was ground using 400-, 600-, 800-, 1000-, 2400-, 4000-grit SiC paper and polished with 6 µm, 3 µm and 1 µm diamond suspension and OPS (each 15 min). Finally, the cross-sections were finished on a VibroMet 2 device from Buehler (ITW Test & Measurement GmbH, Leinfelden-Echterdingen, Germany) using a mixture of deionized water (300 ml) and a colloidal silica suspension (100 ml, 0.06 µm, MasterMet, Buehler, ITW Test & Measurement GmbH, Leinfelden-Echterdingen, Germany) for 48 h. Each sample was additionally weighted with 400 g during polishing on the VibroMet 2. EBSD measurements were conducted using the field emission scanning electron microscope NEON 40 EsB (Zeiss, Jena, Germany) at 15 kV. The high-current mode and an aperture of 60 µm were used. The working distance was set between 18 mm and 20 mm. The collected data was evaluated with the EDAX OIM Analysis software (AMETEK GmbH, Unterschleissheim, Germany). Cleaning was done with the grain CI standardization (grain tolerance angle 15.0°, minimum grain size 5, multi-row required). Transmission electron microscopy (TEM) specimens were prepared by using the focused ion beam (FIB) lift-out technique on a Zeiss Crossbeam 540 FIB/SEM, with the sample location indicated in Fig. 1. The defect structure was analyzed by conventional TEM (CTEM) using a Philips CM200 equipped with a LaB_6 cathode, operated at an accelerating voltage of 200 kV. High-resolution scanning TEM (HRSTEM) imaging was performed using a probe Cs-corrected Spectra 200C-FEG from Thermo Fisher Scientific (TFS) at 200 kV. High-angle annular dark-field (HAADF) images were acquired using a semi-convergence angle of 30 mrad and inner and outer detector collection angles of 56–200 mrad. To improve image quality, drift-corrected frame integration (DCFI) was applied, combining 25 individual frames.

3. Results and discussion

3.1. Differential scanning calorimetry (DSC) of ECAP-processed condition C3

In Fig. 2, the differential scanning calorimetry (DSC) thermogram of the ECAP-processed condition C3 is shown. The tested sample was heated and cooled three times up to 1000 °C. The deviation of the heat flow at the beginning and the end of the heating and cooling cycles is due to the inertia of the sample during testing.

In the first heating cycle, two exothermic peaks (I and II) were observed. The second and third heating cycles show a much smaller exothermic peak I, while peak II fully disappears. In the cooling cycles, no peaks appear, which indicates that no phase transformation takes place during heating or that the amount of the formed phase(s) is too small to see the reconversion during cooling. The first exothermic peak ranges from 450 °C to 650 °C with a peak temperature of 583 °C. In contrast, the second exothermic peak is present between 680 °C and 760 °C and the peak temperature is at 718 °C. As the second peak is only present in the first heating cycle, and considering the literature [13,14] and own preliminary studies, this peak is attributed to a recrystallization process. In contrast, the first peak is present in all heating cycles. However, its intensity is reduced with an increasing number of heating cycles. The first peak might be due to microstructural changes, e.g., a phase transformation.

After the DSC measurements, the temperature range between 450 °C and 650 °C seems to be interesting for further mechanical investigations due to the assumed microstructural changes. For further studies, condition C3 was heat treated at 600 °C for 1 h. This temperature was chosen instead of the peak temperature to ensure that the microstructural effects are more pronounced than at 583 °C.

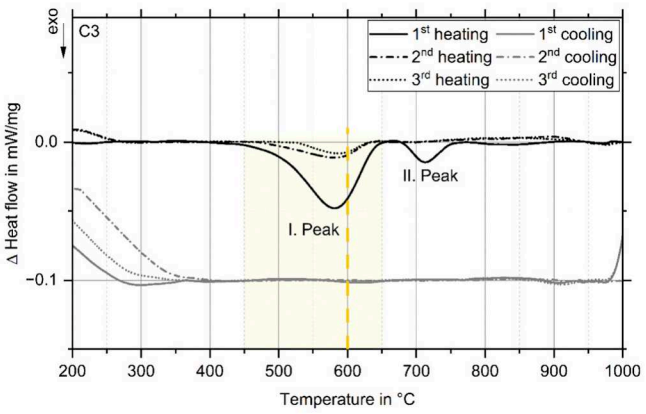

Fig. 2. Differential scanning calorimetry (DSC) thermogram of the ECAP-processed condition C3. The heating/cooling rate was set to 20 K/min. The first exothermic peak (I. Peak) ranges from 450 °C to 650°C, while the second exothermic peak (II. Peak) ranges from 680 °C to 760 °C and is attributed to recrystallization. The first peak might be attributed to a phase transformation, as it is also found during the second and third heating cycles. Therefore, a heat treatment temperature of 600 °C is chosen for further investigations.

3.2. HEXRD measurements

After the heat treatment, crystallographic information of the conditions C0, C3, and C3, 600 °C, 1 h was determined using HEXRD measurements. The HEXRD diffractograms with the identified peak positions assigned to the respective phases are given in Fig. 3.

All tested conditions exhibit a fcc phase, see Fig. 3a. In addition, a small peak next to the (111) plane of the fcc phase is found for conditions C3 and C3, 600 °C, 1 h. This peak might be attributed to the (100) plane of a Co-type hcp-phase. The small hcp peaks indicate that only fine hcp structures are formed as well as small fractions exist. However, the hcp-phase could not be substantiated by additional distinct or standalone peaks. Deng et al. [13,14] reported the formation of a hcp-phase after three ECAP passes and a subsequent heat treatment at 500 °C and 600 °C for 1 h. However, the authors could detect the hcp-phase only by using HR-TEM. In contrast, Praveen et al. [16] did not find a hcp-phase after a heat treatment at 500 °C and 600 °C for 2 min to 1 h using also TEM. It has to be pointed out, if a hcp-phase was reported in literature, it was only a few atomic layers thick, and thus, detection by XRD was not possible [13]. Therefore, in this study synchrotron and HR-TEM investigations were performed to clearly identify the existence of an hcp-phase.

3.3. Quasi-static mechanical properties under tensile loading

The engineering stress-strain curves of the tested conditions C0, C3, and C3, 600 °C, 1 h are shown in Fig. 4a.

Before ECAP processing, condition C0 reaches a yield strength (YS) of (336.9 ± 18.2) MPa and an ultimate tensile strength (UTS) of (785.4 ± 13.2) MPa. The determined YS and UTS of condition C0 are slightly smaller than that of a polycrystalline CrCoNi alloy processed by casting and rotary swaging tested at 20 °C reported in the literature [1]. The difference in YS and UTS is attributed to the larger grain size in the present study (27.78 µm) compared to the grain size of Laplanche et al. [1] (16 µm). The yield-to-tensile ratio was calculated to be 0.43. Such a low yield-to-tensile ratio indicates a high dislocation storage capacity. In addition, condition C0 is characterized by an uniform elongation (UE) of

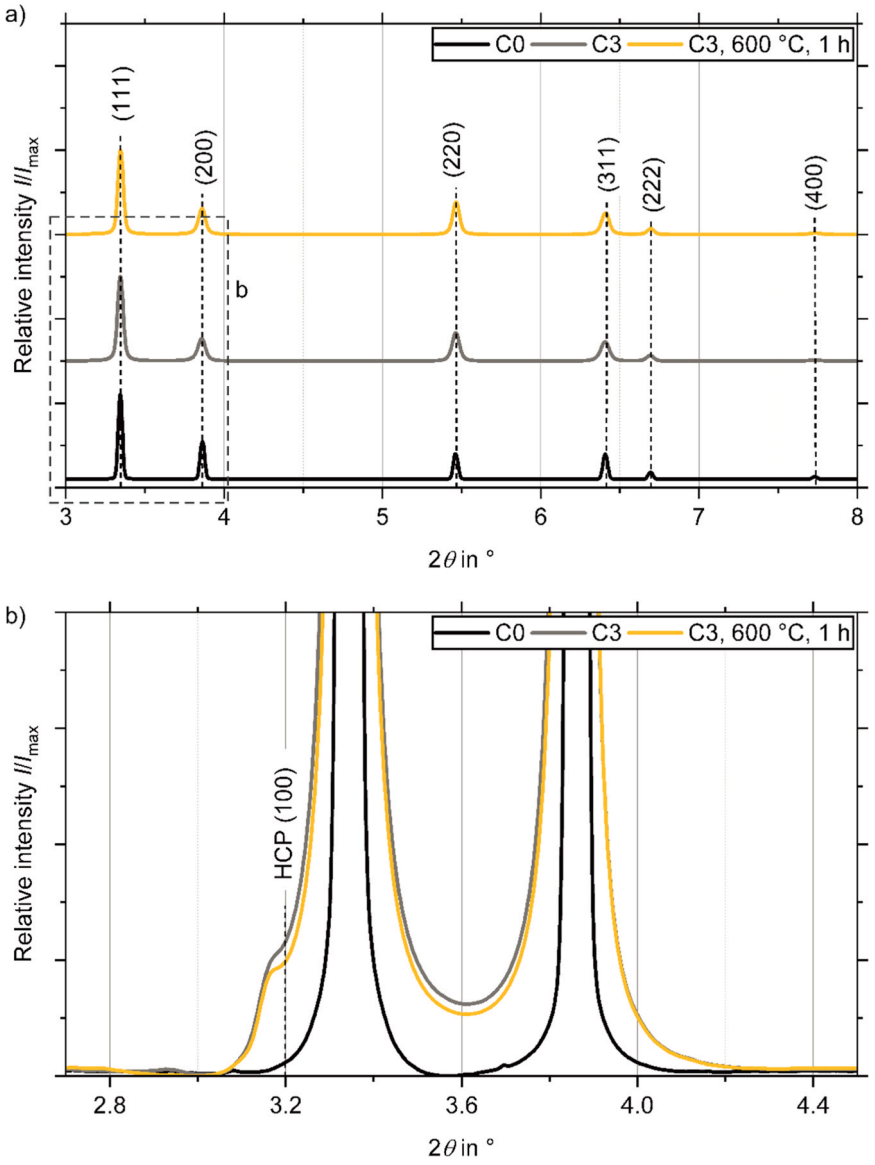

Fig. 3. Diffractogram of the conditions C0, C3, and C3, 600 °C, 1 h obtained by HEXRD analysis. All conditions exhibit a fcc phase (a). In addition, a small peak of a hcp-phase is found for conditions C3 and C3, 600 °C, 1 h (b). However, the hcp-phase is not confirmed by a second peak.

(54.6 ± 2.3)% and an elongation at fracture (EF) of (75.0 ± 0.9)%. After three ECAP passes, YS (1133.4 ± 13.2) MPa and UTS (1241.0 ± 14.0) MPa are significantly increased. The YS and UTS is similar to those found by Deng et al. [13] after three ECAP passes. The YS/UTS ratio is about 0.92, which means that only a few more dislocations can be stored in the microstructure during tensile loading before non-uniform deformation of the material takes place. Furthermore, UE and EF are strongly reduced to about 1.6 %, or, respectively, to less than 21.5 %. It should be mentioned that the UE is very low, which means that necking of the material appears early during straining. Compared to Deng et al., the EF is about 139 % higher. The higher EF might be attributed to the heated ECAP tool during processing (300 °C). Therefore, similar YS and UTS as well as a higher EF are achieved using a processing temperature of 300 °C compared to the study of Deng et al. [13]. This mechanical behavior is therefore typical for ECAP-processed materials and attributed to the strengthening mechanisms of dislocation strengthening and grain boundary strengthening and thus the low dislocation storage capability [18]. In addition, the deformation behavior of CrCoNi under quasi-static tensile load at room temperature is dominated by dislocation glide [1, 19]. ECAP processing introduces a high fraction of dislocations, which hinder each other's glide, leading to the formation of high-density dislocation arrangements (HAAD) and cell structures. Although the complex nature of HEAs/MEAs is due to the equimolar composition of the alloying elements and the thus operating core effects (high configurational entropy, sluggish diffusion, high lattice distortion, and cocktail effect) [7,8], the quasi-static mechanical behavior of CrCoNi is similar to that of conventional alloys, such as aluminum [47] and copper [48]. The significant increase in strength but drastically low uniform elongation was also reported by Deng et al. [13] after ECAP processing and Slone et al. [10] after rolling. It is assumed that the contribution of dislocation strengthening and grain boundary strengthening dominates the quasi-static mechanical behavior of CrCoNi after three ECAP passes at room temperature. Only at lower temperature (77 K), deformation twinning is activated at the same strain rate to enhance the ductility [3, 49]. Interestingly, the YS and UTS of CrCoNi are further increased to YS = 1347.1 ± 16.9 MPa and UTS = 1442.2 ± 9.1 MPa after a heat treatment at 600 °C for 1 h, see Fig. 4a. In contrast, the UE and EF are reduced to (1.2 ± 0.1)% and (16.7 ± 1.4)%, respectively. In Fig. 4b, the corresponding true-stress-strain curves of the tested conditions are given. In addition, condition C3, 600 °C, 1 h fractured at a true stress of

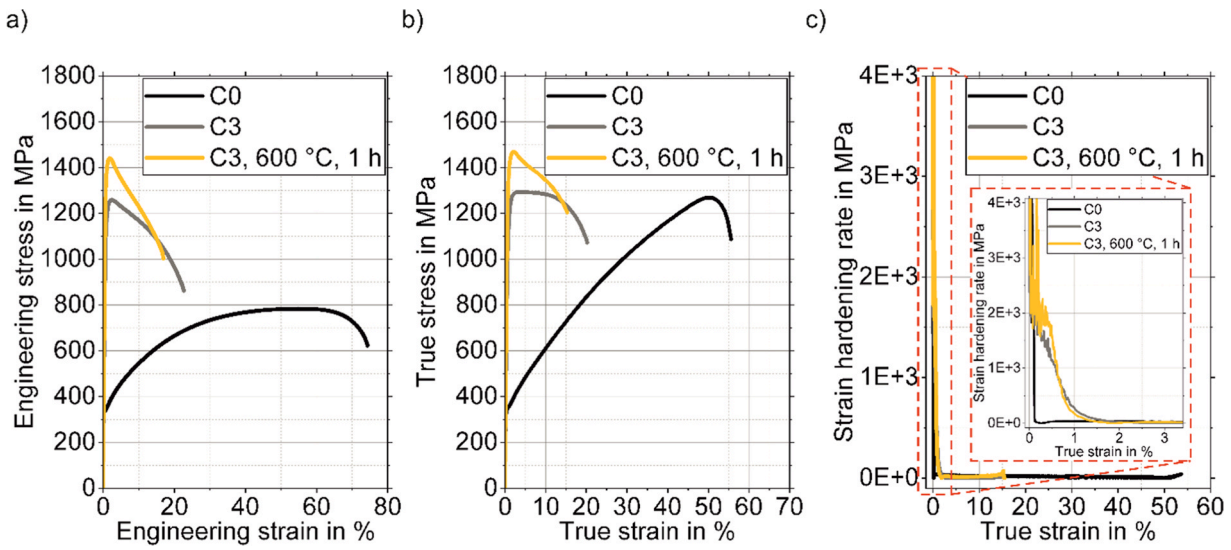

Fig. 4. Results of the quasi-static tensile tests. Engineering stress-strain curves (a), true stress-strain curves (b), and strain hardening curves (c) of the conditions C0, C3, and C3, 600 °C, 1 h. The red dashed rectangle in (c) marks the steep increase of the strain hardening of the conditions C3 and C3, 600 °C, 1 h.

approximately 1.4 GPa, which is about 200 MPa higher than condition C3. However, the true strain at fracture of both conditions is almost similar. The strain hardening curves (Fig. 4c) of conditions C3 and C3, 600 °C, 1 h exhibit a steep increase in the strain hardening rate (marked by the dashed rectangle magnified in Fig. 4c) before it decreases rapidly. In contrast, condition C0 shows a nearly constant strain hardening rate up to higher strains. As mentioned earlier, the mechanisms of dislocation and grain boundary strengthening determine the deformation behavior of ECAP-processed material, despite the complex nature of CrCoNi. Both mechanisms also contribute to the well-known Hall-Petch relationship, as with decreasing grain size, the overall strength of the material increases [50]. In addition, the change in the slope of the strain hardening curve is mostly attributed to a change in the deformation mechanisms. CrCoNi is known to change its deformation mechanisms from dominant planar slip to deformation twinning and phase transformation with increasing strain [1,20], strain rate [21], and decreasing temperature [1,19,20,22,23]. However, it should be noted that three ECAP passes introduced to CrCoNi do not lead to an improved strength-ductility synergy. The mechanisms of dislocation strengthening and grain boundary strengthening dominate the quasi-static mechanical behavior, similar to most metallic materials [1], but other factors can promote strengthening further. The increase in YS and UTS after a severe plastic deformation and a heat treatment between 450 °C and 650 °C of CrCoNi is also mentioned in literature [10,13,14,24,51]. The increase in strength is often explained by the nucleation of a hcp-phase in CrCoNi after a (severe) plastic deformation and a heat treatment in the mentioned temperature range. Deng et al. [14] assumed that the hcp-phase is precipitated after annealing to reduce or eliminate lattice distortion. The nucleation of the hcp-phase in fcc metals with a low stacking fault energy is associated with the introduction of an ISF [20]. Originating from this ISF, a second partial dislocation is activated on a second neighboring plane, leading to the hcp sequence, which grows by adding further partial dislocations. However, the results of the HEXRD measurements in Fig. 3 do not definitely confirm the presence of a hcp-phase in the observed conditions, as only one peak was found. Furthermore, both conditions, C3 and C3, 600 °C, 1 h, exhibit the unknown phase. Therefore, the increase in strength of condition C3, 600 °C, 1 h could not be explained by the formation of an unknown phase. In order to clarify the origin of the increase in strength after ECAP processing and heat treatment in CrCoNi, EBSD, TEM, and high-resolution HAADF STEM investigations are conducted and discussed in the following section.

3.4. Microstructural characterization of condition C0, C3, and C3, 600 °C, 1 h

In order to investigate the microstructure in detail, electron backscatter diffraction (EBSD) measurements were conducted. The orientation (inverse pole figure, IPF) maps in combination with the image quality (IQ) maps are shown in Fig. 5a–c. Furthermore, the IQ maps with the Σ3 (yellow) and Σ9 (red) boundaries are given in Fig. 5d–f. The grain boundaries are marked in black.

The recrystallized condition C0 exhibits equiaxed grains, which are randomly distributed (Fig. 5a). The grain size was determined by EBSD to be (27.78 ± 5.54) μm. The microstructure of C0 is characterized by numerous recrystallization twins (Σ3, Σ9 twins), as shown in the IQ maps in Fig. 5d. After ECAP processing (Fig. 5b), the microstructure is severely deformed, and the mean grain size is reduced to the submicrometer range ((0.25 ± 0.05) μm). The reduced grain size is one cause for the increase in YS and UTS, while UE and EF are drastically reduced (Fig. 4) [18]. In addition, a high number of dislocations is introduced by ECAP processing, which also leads to an increased material strength [18]. As described above, the contributing strengthening mechanisms are grain refinement (Hall-Petch relationship) and dislocation strengthening [18]. After the heat treatment of condition C3 at 600 °C for 1 h, the microstructure appears to be similar to the C3 condition without any further heat treatment (Fig. 5c). The mean grain size slightly increases to (0.30 ± 0.01) μm. The slight increase in grain size might be attributed to the rearrangement and annihilation of dislocations due to recovery processes at 600 °C [16]. In addition, the dislocation density was estimated from the X-ray diffraction peaks determined by HEXRD data and the Scherrer equation $D = K\lambda/(B\cos\theta)$. The crystallite size D is calculated by the Scherrer constant K, which is set to 0.94 for cubic systems, the X-ray wavelength λ (0.12 Å), the line broadening at half of the maximum intensity B, and the Bragg angle θ. From the crystallite size, the dislocation density δ is estimated by $\delta = 1/D^2$. The dislocation density δ was calculated by the mean value of the first four diffraction peaks, as they have the highest intensity. The initial condition C0 exhibits a dislocation density of $(2.7 \bullet 10^{15} \pm 0.3 \bullet 10^{15})$ m^{-2}. After three ECAP passes, the dislocation density is increased to $(8.2 \bullet 10^{15} \pm 2.5 \bullet 10^{15})$ m^{-2}. In contrast, the heat treatment of condition C3 at 600 °C for 1 h leads to a decrease of the dislocation density to $(7.0 \bullet 10^{15} \pm 1.9 \bullet 10^{15})$ m^{-2}. In addition, recrystallization of condition C3, 600 °C, 1 h was not observed, which is in agreement with the findings from the DSC measurements in Fig. 2 and Fig. 4 as recrystallization starts

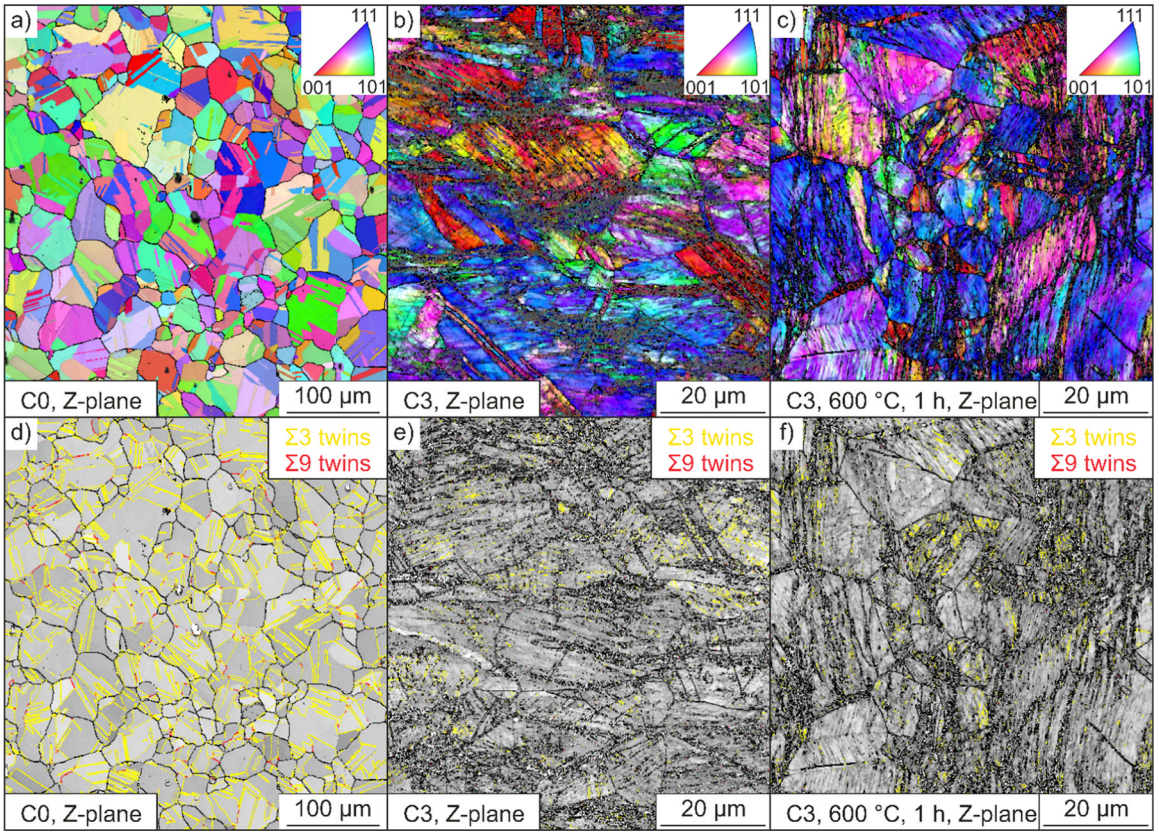

Fig. 5. Orientation (inverse pole figure, IPF) maps in combination with image quality (IQ) maps and high-angle grain boundaries (GB, black) (a–c) as well as IQ maps with GBs (black), Σ3 (yellow), and Σ9 twins (red) (e–f). a),d): Condition C0, b),e): after ECAP C3, c),f): after ECAP and 600°C for 1 h.

above 650 °C. Consequently, no reduction in strength was observed in the stress-strain curves. Furthermore, the fraction of Σ3 and Σ9 twins is reduced from 0.551 ± 0.057 for C0–0.310 ± 0.060 for C3 and 0.292 ± 0.028 for C3, 600 °C, 1 h conditions, as shown in Fig. 5d–f. The following three points potentially explain the observed reduction of the fraction of twins: First, the Σ3 and Σ9 twins in condition C0 (Fig. 5a) are annealing twins, whereas the twins in the other conditions (Fig. 5b, c) are probably deformation twins due to their size and shape. Second, the step size during the EBSD measurements was 50 nm, which means that microstructural features smaller than 50 nm could not be detected by this method. Third, ECAP processing might introduce a twin microstructure, which exhibits misorientations below the used tolerance angle of 5° so that fewer twin boundaries are detected by EBSD. In summary, the decrease in twin fraction between conditions C0, C3 and C3, 600 °C, 1 h could not explain the increase in strength observed in Fig. 4. The increase in strength could not be explained by EBSD measurements. Therefore, TEM investigations and high-resolution HAADF-STEM are further conducted.

In Fig. 6, bright-field TEM images of condition C3 (Fig. 6a, b) and C3, 600 °C, 1 h (Fig. 6c, d) are given. The corresponding selected area diffraction patterns (SAED) are inserted in Fig. 6a (C3) and Fig. 6c (C3, 600 °C, 1 h). The microstructure after three ECAP passes is characterized by a high number of dislocations, which are arranged in HDDAs, see Fig. 6a. In addition, deformation twins/twin bundles were found (marked by yellow arrows in Fig. 6a). In Fig. 6b, the HDDA region is magnified. Inside the HDDA, a network of twins/SFs, which are aligned in two directions, was found (marked by white arrows in Fig. 6b). Similar to the results of the EBSD measurements, the microstructure of condition C3, 600 °C, 1 h (Fig. 6c, d) consists of a high number of dislocations and deformation twins/twin bundles. In literature, SFs and Lomer-Cottrell locks were additionally found after ECAP processing of CrCoNi [13]. Both SAED patterns show a diffraction pattern composed of diffraction spots typical for nanocrystalline materials and also well-known for materials subjected to several ECAP passes. As the grain size of condition C3 was slightly smaller than for condition C3, 600 °C, 1 h, tilting in zone axis {1 1 1} was impossible. In addition, the twin boundaries in condition C3, 600 °C, 1 h appears more planar and defect-free than the twin boundaries in condition C3. It might be that due to the heat treatment, partial dislocations are able to move at the deformation twin boundaries in order to reduce the introduced energy through SPD. If the deformation twin boundaries reach an equilibrium state with a corresponding equilibrium shape, the hindering effect of this twin boundary against dislocation motion is increased, leading to the observed increase in strength.

However, the TEM bright field images do not elucidate the origin of the strength increase due to the heat treatment at 600 °C for 1 h as the given resolution, it is hard to decide whether twins or SFs are present. As a consequence, high-resolution HAADF-STEM investigations were conducted. Unfortunately, it was only able for condition C3, 600 °C, 1 h to tilt in the zone axis {1 1 1}, as the grain size of condition C3 was too small. In addition, condition C3 exhibits a higher dislocation density, which also hinders tilting in the zone axis. After the heat treatment, the dislocation density is reduced and grain boundary relaxation occurs. As a consequence, tilting in zone axis is easier. The corresponding high-resolution HAADF-STEM image of condition C3, 600 °C, 1 h along the zone axis {1 1 1} is given in Fig. 7.

The microstructure comprises twin boundaries, nanotwins, and SFs (Fig. 7a). In Fig. 7b, the stacking sequence of a nanotwin is magnified. The stacking sequence confirms that there is no phase transformation in the microstructure as described in literature [13–15]. However, it should also be taken into account that due to the small area, which was investigated during high-resolution HAADF-STEM, small lattice defects, such as the hcp stacking sequence, could be missed.

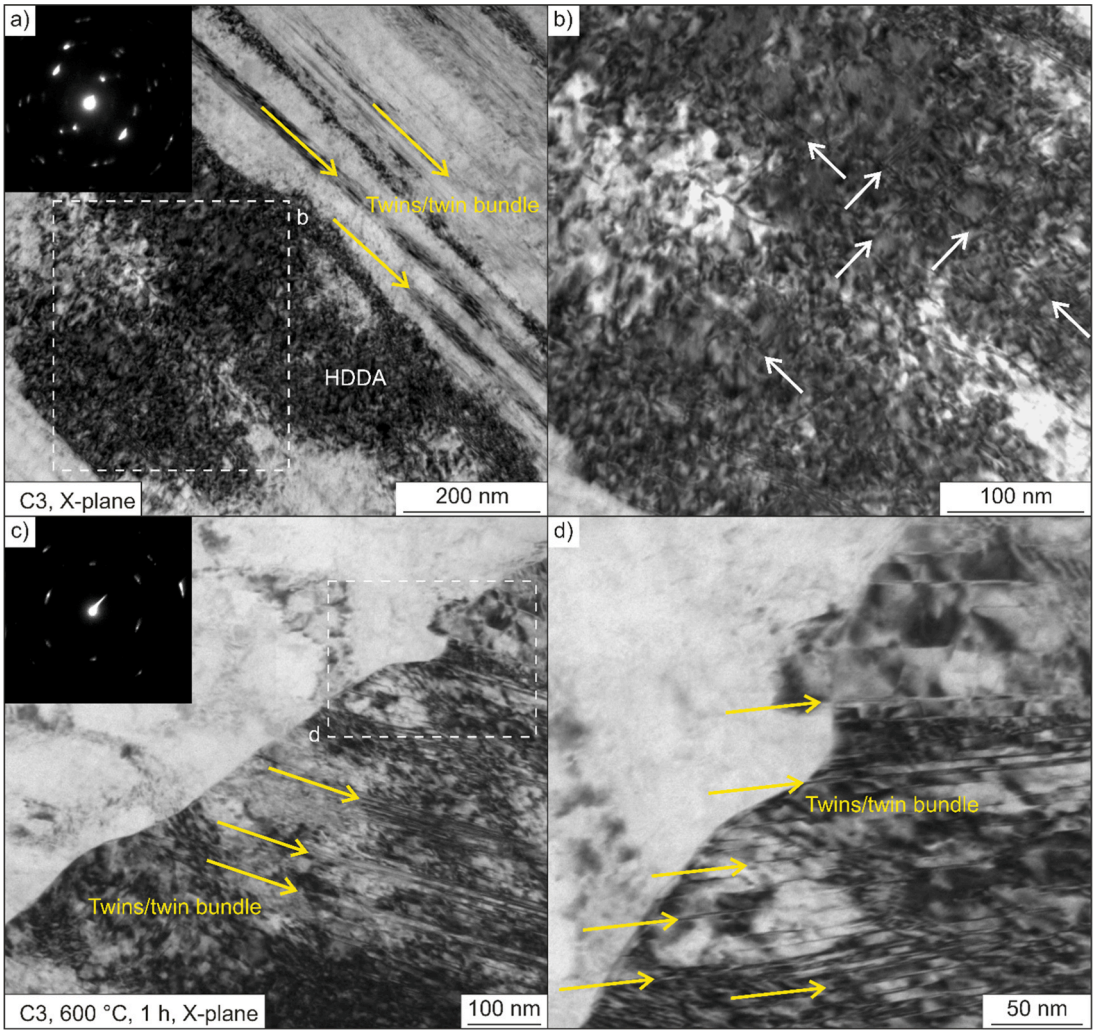

Fig. 6. Bright-field images (TEM) and selected area electron diffraction (SAED) pattern of the condition C3 (a, b) and C3, 600 °C, 1 h (c, d). After ECAP processing, high-density dislocation arrangements (HDDA) and twins/twin bundles (yellow arrows) are observed (a). In (b), the area of HDDA is magnified, and some twins/SFs were found (white arrows). After a heat treatment at 600 °C for 1 h, the microstructure appears similar to that after three ECAP passes. The given resolution it is hard to decide whether twins or SFs are present. Thus high-angle annular dark-field (HAADF)-STEM (Fig. 7) investigations have been performed. The sample area contributing to the SAED pattern was approximately 1–2 μm².

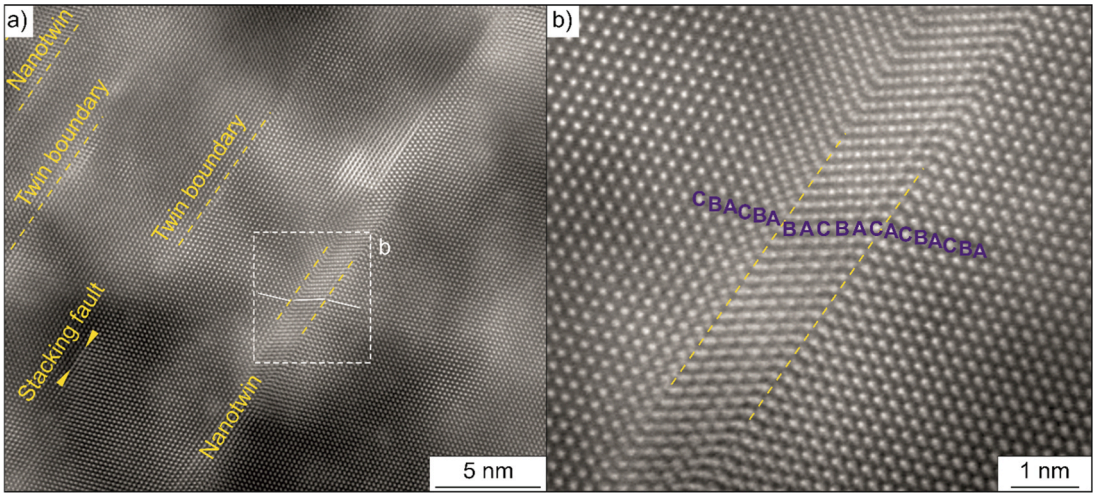

Fig. 7. High-resolution HAADF-STEM image of condition C3, 600 °C, 1 h along the zone axis {1 1 1}. The microstructure comprises nanotwins and twin boundaries as well as SFs (a). The magnified area in (b) shows the stacking sequence of the observed nanotwin.

To summarize the observed results of this study, the origin of the increase in strength from C3 to C3, 600 °C, 1 h conditions could not be finally clarified by HEXRD, TEM, and high-resolution HAADF-STEM investigations. In addition, further TEM and/or high-resolution HAADF-STEM investigations will not improve the understanding of the microstructural origin of the observed mechanical behavior of conditions C3 and C3, 600 °C, 1 h, as the severely plastically deformed, ultrafine-grained microstructure is not suitable for tilting in the desired zone axis, and the high dislocation density impedes the identification of other potentially acting microstructural elements such as hcp-phase transformation or SRO. The often-mentioned reason in literature, the transformation from fcc to hcp at the twin boundaries, is not confirmed in this study. Consequently, the increase in material's strength has to be attributed to another mechanism. At room temperature, the dominating deformation mechanism in CrCoNi is dislocation glide [1,19]. Therefore, the interaction of dislocations plays a significant role during the deformation process of severely plastically deformed microstructures, e. g., after ECAP processing, as they exhibit a high dislocation density. As described under 3.3, the YS/UTS ratio of condition C3 was calculated to be 0.92, which means that only a few more dislocations can be stored before necking of the material occurs. In literature, another mechanism is described, which might explain the increase in strength of nanostructured materials without a significant change in grain size or a phase transformation [34]. The so-called "anneal-induced hardening" [16,30,33,52] or "anneal hardening" [31] might be caused by the relaxation of grain boundaries and segregation of alloying elements at the grain/twin boundaries. The driving force for segregation is to minimize the planar fault energy [53,54]. Both effects hinder grain boundary sliding [33]. Another possible reason described for ultrafine-grained materials after SPD is the annihilation of mobile dislocations and the rearrangement of remaining dislocations in low-energy configurations, e.g., low-angle grain boundaries and dipolar dislocation walls [33,43]. Sheinermann [32] suggest a model for annealing-induced hardening in ultrafine-grained metals. They explain the increase in material's strength in ultrafine-grained microstructures after low-temperature annealing due to the relaxation of grain boundaries by a decrease in the number of grain boundary dislocation sources. As a consequence, a higher load is required to activate the hardened grain boundary dislocation sources and/or the same dislocation sources again, leading to the increase in strength. In addition, Ge et al. [43] reported that the rearrangement of dislocations leads to the formation of nano-subgrains in the deformation-induced shear bands and an enhanced back-stress strengthening of an FeCoNi-based MEA. Both promote the annihilation of mobile dislocations, resulting in hardening of the material. Therefore, a small decrease in the dislocation density as observed for conditions C3 and C3, 600 °C, 1 h from $2.5 \bullet 10^{15}$ m^{-2} to $2.0 \bullet 10^{15}$ m^{-2} might be an indicator for anneal hardening. However, clear nano-subgrain structures within shear bands, in which plastic deformation is localized, have not been detected. Although HDDAs were found by TEM studies (Fig. 6), which indicate strong dislocation activities during straining.

Furthermore, Wessels et al. [35] propose another idea to explain the increase in material strength of ultrafine-grained metals after low-temperature annealing. During pre-deformation, multiple slip occurs in the grains, resulting in the formation of long jogs on forest dislocations and numerous vacancies. During annealing of the material, the jogs climb out of the active slip plane. If the material is then plastically deformed, e.g., during tensile testing, the gliding dislocations cross the un-jogged forest dislocations in the active slip plane, which increases the UTS. However, this assumption does not explain the increase in YS. Therefore, it is assumed that the formation of jogs on forest dislocations is not the origin of the observed material behavior. The increase in material's strength for HEAs/MEAs is sometimes also explained in literature by short-range ordering (SRO) [27–29].

Taking into account the above-mentioned findings from literature and based on our own results regarding the increase in strength after a heat treatment the following picture can be drawn:

On the one hand, HEXRD and HAADF-STEM give no proof that SRO has taken place, albeit further investigations by scanning electron nanodiffraction or extended X-ray absorption fine structure analysis may allow for deeper insights. However, based on the findings SRO is either absent or is considered not to be pronounced enough to account for the observed hardening. On the other hand, HEXRD reveals a weak hcp-related peak for conditions C3 and C3, 600 °C, 1. Thus, it is assumed that the hcp-phase is nucleated in very fine structures, e. g., as mentioned in the literature, at deformation twin boundaries for a few atomic layers, and in small fractions. In fcc-materials, a hcp-phase can be formed from ISFs and/or twin boundaries only by the glide of a partial dislocation [20,26]. Therefore, the formation of a hcp-phase is energetically favored in CrCoNi. The presence of nanotwins and ISF is confirmed by high-resolution HAADF-STEM investigations. It was also found that the strain hardening rates of both ECAP-processed conditions are quite similar, but a bit more pronounced for condition C3, 600 °C, 1 h (see Fig. 4c). The slightly reduced dislocation density of condition C3, 600 °C, 1 h might lead to a stronger interaction between mobile dislocations and ISF as well as twin boundaries instead of dislocation-dislocation interactions. In addition, the twin boundaries of condition C3, 600 °C, 1 h appear to be more planar and defect-free, which will also increase their resistance against dislocation glide. However, as the differences in the strain hardening rates are small when compared to condition C3, the main difference in strength has to be linked to the onset of plastic deformation. The YS and UTS of condition C3, 600 °C, 1 h are approximately 200 MPa higher than the YS and UTS of condition C3. In addition, the dislocation density was only slightly reduced by the annealing and is still at a high level. From this point of view, the rearrangement of dislocations in low-energy configurations [55] and, to some extent, the grain boundary relaxation [16,30–33] both introduced by the subsequent heat treatment, are considered to be the cause of the strong increase in YS and UTS. It is suggested that after the heat treatment, dislocations are incorporated in grain and twin boundaries during straining [44]. Such fully incorporated dislocations become immobile, which directly generate lattice distortions and a corresponding stress field. Therefore, higher stresses are needed for further straining of the material. In other words, the annealing after three ECAP passes has strongly affected the dislocation sourcing mechanism, either by hindering dislocations from bowing out or by activating new sources. As the grain size is in the ultra-fine-grained regime and the dislocation density is still high, it is rather likely to suppose that dislocations bowing out from the grain boundaries govern the yielding behavior; compare Mompiou et al. [44]. The hardening by annealing effect can thus be attributed to the relaxation of the grain boundaries (including twin boundaries) and shifting the stresses needed for bowing out of grain boundary dislocations to a higher stress level. Despite the complex nature of CrCoNi and the mentioned core effects in the literature, the dominating deformation mechanism is still dislocation glide, and the material is strengthened by dislocation and grain boundary strengthening, similar to most metallic materials after ECAP processing.

4. Conclusion

In this study, the influence of ECAP processing and a heat treatment on the medium-entropy alloy CrCoNi was investigated. The initial recrystallized condition (C0) was subjected to three ECAP passes (C3). In addition, condition C3 was then subsequently heat treated at 600 °C for 1 h (C3, 600 °C, 1 h) under an argon atmosphere. The study focuses on the microstructural evolution due to ECAP processing and a heat treatment as well as the resulting mechanical properties. The findings are summarized as follows:

– After 3 ECAP passes, two exothermic peaks were found in the DSC thermogram. The first peak between 450 °C and 650 °C could not be attributed to a specific microstructural change. In contrast, the

second exothermic peak between 680 °C and 760 °C is attributed to the recrystallization of the severely deformed microstructure.
- HEXRD measurements determined a shoulder of an unknown phase for conditions C3 and C3, 600 °C, 1 h that could be attributed to an hcp-phase: However, one peak is not enough to determine a phase significantly.
- 3 ECAP passes in combination with a heat treatment at 600 °C for 1 h (in the temperature range of the first exothermic peak found by DSC) lead to an increase in YS and UTS while UE and EF are decreased.
- EBSD, TEM, and high-resolution HAADF-STEM investigations revealed no significant changes of the microstructure between condition C3 and C3, 600 °C, 1 h. Both microstructures comprise small grains, high-density dislocation arrangements, nanotwins, and SFs.
- CrCoNi shows similar quasi-static mechanical behavior as conventional alloys after ECAP processing and a subsequent heat treatment. It is dominated by dislocation interactions and thus does not overcome the strength-ductility trade-off.
- The increase in YS and UTS is attributed to the rearrangement of dislocations in low-energy configurations and, to some extent, to grain and twin boundary relaxation. The anneal-induced hardening effect at 600 °C seems to be related to a shift of the stress needed for bowing out grain boundary dislocations and to activate new dislocation sources to a higher stress level, resulting in the observed higher YS and UTS.

CRediT authorship contribution statement

Thomas Lampke: Supervision, Resources, Funding acquisition. **Lisa Winter:** Writing – review & editing, Investigation, Formal analysis. **Andreas Stark:** Writing – review & editing, Methodology, Investigation, Formal analysis. **Nina Pfeffer:** Writing – review & editing, Methodology, Investigation, Formal analysis. **Patrick Ortner:** Writing – review & editing, Methodology, Investigation, Formal analysis. **Heinz Werner Höppel:** Writing – review & editing, Supervision, Resources, Methodology, Investigation, Formal analysis, Conceptualization. **Lisa-Marie Rymer:** Writing – original draft, Methodology, Investigation, Formal analysis, Conceptualization.

Funding

This work was funded by the Deutsche Forschungsgemeinschaft (DFG, German Research Foundation) – project number 468469638.

Declaration of Competing Interest

The authors declare that they have no known competing financial interests or personal relationships that could have appeared to influence the work reported in this paper.

Acknowledgements

The authors thank CMMC GmbH for conducting the hot forging, Thomas Senß for performing the heat treatments, Tom Petschowsky for ECAP processing, Max Müller for conducting the DSC measurements, Felix Schubert for performing the quasi-static tensile tests, Viktoriia Chzhan, Jenny Roßmann and Sebastian Hofmann for preparing the cross-sections for microstructural characterization, and Jan Vollhüter for the preparation of the FIB lamellae. In addition, the authors acknowledge the Deutsches Elektronen Synchrotron, DESY (Hamburg, Germany), member of the Helmholtz Association HGF, for providing the experimental facilities. The HEXRD measurements in this study were performed at PETRA III/P07-High Energy Materials Science beamline. Beamtime was allocated for proposal I-20230881. The HRTEM measurements in this study were performed at the CENEM Erlangen.

Data availability

Data will be made available on request.

References

[1] G. Laplanche, A. Kostka, C. Reinhart, J. Hunfeld, G. Eggeler, E.P. George, Reasons for the superior mechanical properties of medium-entropy CrCoNi compared to high-entropy CrMnFeCoNi, Acta Mater. 128 (2017) 292–303, https://doi.org/10.1016/j.actamat.2017.02.036.
[2] M. Schneider, E.P. George, T.J. Manescau, T. Záležák, J. Hunfeld, A. Dlouhý, G. Eggeler, G. Laplanche, Analysis of strengthening due to grain boundaries and annealing twin boundaries in the CrCoNi medium-entropy alloy, Int J. Plast. 124 (2020) 155–169, https://doi.org/10.1016/j.ijplas.2019.08.009.
[3] B. Gludovatz, A. Hohenwarter, K.V.S. Thurston, H. Bei, Z. Wu, E.P. George, R. O. Ritchie, Exceptional damage-tolerance of a medium-entropy alloy CrCoNi at cryogenic temperatures, Nat. Commun. 7 (2016), https://doi.org/10.1038/ncomms10602.
[4] D. Liu, Q. Yu, S. Kabra, M. Jiang, P. Forna-Kreutzer, R. Zhang, M. Payne, F. Walsh, B. Gludovatz, M. Asta, A.M. Minor, E.P. George, R.O. Ritchie, Exceptional fracture toughness of CrCoNi-based medium- and high-entropy alloys at 20 kelvin, Science (1979) 378 (2022) 978–983, https://doi.org/10.1126/science.abp807.
[5] A. Wetzel, M. von der Au, P.M. Dietrich, J. Radnik, O. Ozcan, J. Witt, The comparison of the corrosion behavior of the CrCoNi medium entropy alloy and CrMnFeCoNi high entropy alloy, Appl. Surf. Sci. 601 (2022), https://doi.org/10.1016/j.apsusc.2022.154171.
[6] C. Stephan-Scherb, W. Schulz, M. Schneider, S. Karafiludis, G. Laplanche, High-temperature oxidation in dry and humid atmospheres of the equiatomic CrMnFeCoNi and CrCoNi High- and medium-entropy alloys, Oxid. Met 95 (2021) 105–133, https://doi.org/10.1007/s11085-020-10014-7.
[7] D.B. Miracle, O.N. Senkov, A critical review of high entropy alloys and related concepts, Acta Mater. 122 (2017) 448–511, https://doi.org/10.1016/j.actamat.2016.08.081.
[8] R.S. Mishra, R.S. Haridas, P. Agrawal, High entropy alloys – Tunability of deformation mechanisms through integration of compositional and microstructural domains, Mater. Sci. Eng. A. 812 (2021), https://doi.org/10.1016/j.msea.2021.141085.
[9] P. Sathiyamoorthi, P. Asghari-Rad, J.W. Bae, H.S. Kim, Fine tuning of tensile properties in CrCoNi medium entropy alloy through cold rolling and annealing, Intermet. (Barking) 113 (2019), https://doi.org/10.1016/j.intermet.2019.106578.
[10] C.E. Slone, J. Miao, E.P. George, M.J. Mills, Achieving ultra-high strength and ductility in equiatomic CrCoNi with partially recrystallized microstructures, Acta Mater. 165 (2019) 496–507, https://doi.org/10.1016/j.actamat.2018.12.015.
[11] Z. Zhang, Y. Wu, L. Bhatta, C. Li, B. Gan, C. Kong, Y. Wang, H. Yu, Mechanical properties and microstructure evolution of a CrCoNi medium entropy alloy subjected to asymmetric cryorolling and subsequent annealing, Mater. Today Commun. 26 (2021), https://doi.org/10.1016/j.mtcomm.2020.101776.
[12] Y. Wu, Z. Zhang, Y. Zhang, C. Kong, H. Yu, Twinning susceptibility of CrCoNi medium entropy alloy to cryogenic temperature during asymmetric rolling, J. Mater. Res. Technol. 20 (2022) 2638–2649, https://doi.org/10.1016/j.jmrt.2022.08.045.
[13] H.W. Deng, Z.M. Xie, B.L. Zhao, Y.K. Wang, M.M. Wang, J.F. Yang, T. Zhang, Y. Xiong, X.P. Wang, Q.F. Fang, C.S. Liu, Tailoring mechanical properties of a CoCrNi medium-entropy alloy by controlling nanotwin-HCP lamellae and annealing twins, Mater. Sci. Eng. A. 744 (2019) 241–246, https://doi.org/10.1016/J.MSEA.2018.11.143.
[14] H.W. Deng, K. Jing, W.Y. Du, Z.Y. Liu, Z.M. Xie, T. Zhang, H. Li, B. Liu, The annealing induced formation of epsilon martensite in CoCrNi medium-entropy alloy after severe plastic deformation, J. Alloy. Compd. 899 (2022), https://doi.org/10.1016/j.jallcom.2021.163349.
[15] H.W. Deng, H.E. Ge, C.Y. Zhan, Y. Liu, Q.S. Ren, Z.Y. Liu, T. Zhang, Temperature dependence of the deformation behavior and mechanical response of CoCrNi medium-entropy alloy: experiment and simulation, J. Mater. Res. Technol. 24 (2023) 9731–9742, https://doi.org/10.1016/j.jmrt.2023.05.173.
[16] S. Praveen, J.W. Bae, P. Asghari-Rad, J.M. Park, H.S. Kim, Annealing-induced hardening in high-pressure torsion processed CoCrNi medium entropy alloy, Mater. Sci. Eng. A. 734 (2018) 338–340, https://doi.org/10.1016/j.msea.2018.07.107.
[17] P. Sathiyamoorthi, J. Moon, J.W. Bae, P. Asghari-Rad, H.S. Kim, Superior cryogenic tensile properties of ultrafine-grained CoCrNi medium-entropy alloy produced by high-pressure torsion and annealing, Scr. Mater. 163 (2019) 152–156, https://doi.org/10.1016/j.scriptamat.2019.01.016.
[18] M.J. Starink, Dislocation versus grain boundary strengthening in SPD processed metals: non-causal relation between grain size and strength of deformed polycrystals, Mater. Sci. Eng. A. 705 (2017) 42–45, https://doi.org/10.1016/j.msea.2017.08.069.
[19] Z. Zhang, H. Sheng, Z. Wang, B. Gludovatz, Z. Zhang, E.P. George, Q. Yu, S.X. Mao, R.O. Ritchie, Dislocation mechanisms and 3D twin architectures generate exceptional strength-ductility-toughness combination in CrCoNi medium-entropy alloy, Nat. Commun. 8 (2017), https://doi.org/10.1038/ncomms14390.
[20] H. He, M. Naeem, F. Zhang, Y. Zhao, S. Harjo, T. Kawasaki, B. Wang, X. Wu, S. Lan, Z. Wu, W. Yin, Y. Wu, Z. Lu, J.J. Kai, C.T. Liu, X.L. Wang, Stacking fault driven phase transformation in CrCoNi medium entropy alloy, Nano Lett. 21 (2021) 1419–1426, https://doi.org/10.1021/acs.nanolett.0c04244.

[21] S. Zhao, S. Yin, X. Liang, F. Cao, Q. Yu, R. Zhang, L. Dai, C.J. Ruestes, R.O. Ritchie, A.M. Minor, Deformation and failure of the CrCoNi medium-entropy alloy subjected to extreme shock loading, Sci. Adv. 9 (2023), https://doi.org/10.1126/sciadv.adf8602.
[22] M. Naeem, H. Zhou, H. He, S. Harjo, T. Kawasaki, S. Lan, Z. Wu, Y. Zhu, X.L. Wang, Martensitic transformation in CrCoNi medium-entropy alloy at cryogenic temperature, Appl. Phys. Lett. 119 (2021) 1ENG, https://doi.org/10.1063/5.0067268.
[23] P. Gao, Z. Ma, J. Gu, S. Ni, T. Suo, Y. Li, M. Song, Y.W. Mai, X. Liao, Exceptional high-strain-rate tensile mechanical properties in a CrCoNi medium-entropy alloy, Sci. China Mater. 65 (2022) 811–819, https://doi.org/10.1007/s40843-021-1798-6.
[24] B. Schuh, B. Völker, J. Todt, K.S. Kormout, N. Schell, A. Hohenwarter, Influence of annealing on microstructure and mechanical properties of a nanocrystalline CrCoNi medium-entropy alloy, Materials 11 (2018), https://doi.org/10.3390/ma11050662.
[25] S. Sun, W. Zai, Y. Chen, L. Zhao, G. Sun, J. Hu, S. Han, J. Lian, Effects of cold-rolling and subsequent annealing on the nano-mechanical and creep behaviors of CrCoNi medium-entropy alloy, Mater. Sci. Eng. A. 839 (2022), https://doi.org/10.1016/j.msea.2022.142802.
[26] C. Niu, C.R. LaRosa, J. Miao, M.J. Mills, M. Ghazisaeidi, Magnetically-driven phase transformation strengthening in high entropy alloys, Nat. Commun. 9 (2018), https://doi.org/10.1038/s41467-018-03846-0.
[27] Q.J. Li, H. Sheng, E. Ma, Strengthening in multi-principal element alloys with local-chemical-order roughened dislocation pathways, Nat. Commun. 10 (2019), https://doi.org/10.1038/s41467-019-11464-7.
[28] W.R. Jian, Z. Xie, S. Xu, Y. Su, X. Yao, I.J. Beyerlein, Effects of lattice distortion and chemical short-range order on the mechanisms of deformation in medium entropy alloy CoCrNi, Acta Mater. 199 (2020) 352–369, https://doi.org/10.1016/j.actamat.2020.08.044.
[29] Y. Tian, F. Chen, Short-range order-dependent dislocation mobilities in CrCoNi medium entropy alloy: atomistic simulations and modeling, Int J. Plast. 172 (2024), https://doi.org/10.1016/j.ijplas.2023.103859.
[30] Y. Xiao, Y. Li, A. Kostka, M. Rajkowski, M. Schneider, G. Eggeler, G. Laplanche, Annealing-induced hardening in single-phase FCC, equiatomic CrCoNi and non-equiatomic CrCoNiMo medium-entropy alloys, J. Mater. Res. Technol. 30 (2024) 4762–4776, https://doi.org/10.1016/j.jmrt.2024.04.188.
[31] O. Renk, R. Pippan, Anneal hardening in single phase nanostructured metals, Mater. Trans. 64 (2023) 1464–1473, https://doi.org/10.2320/matertrans.MT-MF2022029.
[32] A.G. Sheinerman, S.A. Krasnitckii, A model for annealing-induced hardening in ultrafine-grained metals, Mater. Phys. Mech. 47 (2021) 608–612, https://doi.org/10.18149/MPM.4742021_8.
[33] J. Gubicza, Annealing-induced hardening in ultrafine-grained and nanocrystalline materials, Adv. Eng. Mater. 22 (2020), https://doi.org/10.1002/adem.201900507.
[34] X. Huang, N. Hansen, N. Tsuji, Hardening by annealing and softening by deformation in nanostructured metals, Science (1979) 312 (2006) 249–251, https://doi.org/10.1126/science.1124268.
[35] E.J.H. Wessels, F.R.N. Nabarro, A theory of unstable glide in the presence of a dense dislocation forest, Acta Met. 19 (1971) 915–921, https://doi.org/10.1016/0001-6160(71)90084-8.
[36] M. Mizuno, H. Araki, Structural evolution of short-range order in CrCoNi and MnCoNi medium-entropy alloys, Phys. Rev. Mater. 8 (2024), https://doi.org/10.1103/PhysRevMaterials.8.013601.
[37] H.W. Hsiao, R. Feng, H. Ni, K. An, J.D. Poplawsky, P.K. Liaw, J.M. Zuo, Data-driven electron-diffraction approach reveals local short-range ordering in CrCoNi with ordering effects, Nat. Commun. 13 (2022), https://doi.org/10.1038/s41467-022-34335-0.
[38] X. Yang, Y. Xi, C. He, H. Chen, X. Zhang, S.T. Tu, Chemical short-range order strengthening mechanism in CoCrNi medium-entropy alloy under nanoindentation, Scr. Mater. 209 (2022), https://doi.org/10.1016/j.scriptamat.2021.114364.
[39] S. Shuang, Y. Hu, X. Li, F. Yuan, G. Kang, H. Gao, X. Zhang, Tuning chemical short-range order for simultaneous strength and toughness enhancement in NiCoCr medium-entropy alloys, Int J. Plast. 177 (2024), https://doi.org/10.1016/j.ijplas.2024.103980.
[40] A. Tamm, A. Aabloo, M. Klintenberg, M. Stocks, A. Caro, Atomic-scale properties of Ni-based FCC ternary, and quaternary alloys, Acta Mater. 99 (2015) 307–312, https://doi.org/10.1016/j.actamat.2015.08.015.
[41] J. Ding, Q. Yu, M. Asta, R.O. Ritchie, Tunable stacking fault energies by tailoring local chemical order in CrCoNi medium-entropy alloys, Proc. Natl. Acad. Sci. USA 115 (2018) 8919–8924, https://doi.org/10.1073/pnas.1808660115.
[42] X.Y. Zhang, Q. Liu, X.L. Wu, A.W. Zhu, Work softening and annealing hardening of deformed nanocrystalline nickel, Appl. Phys. Lett. 93 (2008), https://doi.org/10.1063/1.3062849.
[43] P. Ge, K. Gan, D. Yan, P. Wu, W. Wu, Z. Li, Elucidating the origination of annealing-induced hardening in an equiatomic medium-entropy alloy, Adv. Eng. Mater. 25 (2023), https://doi.org/10.1002/adem.202201153.
[44] F. Mompiou, D. Caillard, M. Legros, H. Mughrabi, In situ TEM observations of reverse dislocation motion upon unloading in tensile-deformed UFG aluminium, Acta Mater. 60 (2012) 3402–3414, https://doi.org/10.1016/j.actamat.2012.02.049.
[45] V.M. Segal, Materials processing by simple shear, A (1995), https://doi.org/10.1016/0921-5093(95)09705-8.
[46] M. Furukawa, Y. Iwahashi, Z. Horita, M. Nemoto, T.G. Langdon, The shearing characteristics associated with equal-channel angular pressing, Mater. Sci. Eng. A. 257 (1998) 328–332, https://doi.org/10.1016/S0921-5093(98)00750-3.
[47] W. Abdel-Aziem, A. Hamada, T. Makino, M.A. Hassan, Micro/Meso-scale equal channel angular pressing of Al 1070 alloy: microstructure and mechanical properties, J. Mater. Eng. Perform. 29 (2020) 6201–6211, https://doi.org/10.1007/s11665-020-05090-4.
[48] Y.Z. Tian, Q.Q. Duan, H.J. Yang, H.F. Zou, G. Yang, S.D. Wu, Z.F. Zhang, Effects of route on microstructural evolution and mechanical properties of Cu-8 Wt Pct Ag alloy processed by equal channel angular pressing, Met. Mater. Trans. A Phys. Met. Mater. Sci. 41 (2010) 2290–2303, https://doi.org/10.1007/s11661-010-0313-4.
[49] J. Miao, C.E. Slone, T.M. Smith, C. Niu, H. Bei, M. Ghazisaeidi, G.M. Pharr, M. J. Mills, The evolution of the deformation substructure in a Ni-Co-Cr equiatomic solid solution alloy, Acta Mater. 132 (2017) 35–48, https://doi.org/10.1016/j.actamat.2017.04.033.
[50] L. Zhu, G. Li, W. Dong, J. Zhang, Y. Ma, H. He, S. Lan, Z. Wu, X. Li, T. Yang, X. L. Wang, On the grain size dependence of competing deformation mechanisms in a CrCoNi medium entropy alloy, Acta Mater. 289 (2025), https://doi.org/10.1016/j.actamat.2025.120907.
[51] C.X. Shi, X.H. Du, J.Y. Zhang, G.S. Duan, M.C. Yang, R.F. Zu, W.P. Li, T.H. Chou, B. L. Wu, J. Sun, J.C. Huang, Superb strength-ductility synergy in a medium-entropy CoCrNi alloy via reinforced TRIP effect, J. Mater. Res. Technol. 20 (2022) 104–113, https://doi.org/10.1016/j.jmrt.2022.07.060.
[52] L.X. Sun, N.R. Tao, M. Kuntz, J.Q. Yu, K. Lu, Annealing-induced hardening in a nanostructured low-carbon steel prepared by using dynamic plastic deformation, J. Mater. Sci. Technol. 30 (2014) 731–735, https://doi.org/10.1016/j.jmst.2014.03.008.
[53] H. Suzuki, Chemical interaction of solute atoms with dislocations, science reports of the research institutes, Tohoku University, Ser. A Phys. Chem. Metall. 4 (1952) 455–463.
[54] H. Suzuki, Segregation of solute atoms to stacking faults, J. Phys. Soc. Jpn. 17 (1962) 322–325, https://doi.org/10.1143/JPSJ.17.322.
[55] J. Gubicza, P.H.R. Pereira, G. Kapoor, Y. Huang, S.S. Vadlamani, T.G. Langdon, Annealing-induced hardening in ultrafine-grained Ni–Mo alloys, Adv. Eng. Mater. 20 (2018), https://doi.org/10.1002/adem.201800184.